



Optics Letters

Seamless multi-reticle photonics

WARREN JIN,^{1,2} AVI FESHALI,² MARIO PANICCIA,² AND JOHN E. BOWERS^{1,*}

¹ECE Department, University of California, Santa Barbara, Santa Barbara, California 93106, USA

²Anello Photonics, Santa Clara, California 95054, USA

*Corresponding author: bowers@ece.ucsb.edu

Received 8 April 2021; revised 21 May 2021; accepted 26 May 2021; posted 26 May 2021 (Doc. ID 427289); published 15 June 2021

While Moore's law predicted shrinking transistors would enable exponential scaling of electronic circuits, the footprint of photonic components is limited by the wavelength of light. Thus, future high-complexity photonic integrated circuits (PICs) such as petabit-per-second transceivers, thousand-channel switches, and photonic quantum computers will require more area than a single reticle provides. In our novel approach, we overlay and widen waveguides in adjacent reticles to stitch a smooth transition between misaligned exposures. In SiN waveguides, we measure ultralow loss of 0.0004 dB per stitch, and produce a stitched delay line 23 m in length. We extend the design to silicon channel waveguides, and predict 50-fold lower loss or 50-fold smaller footprint versus a multimode-waveguide-based method. Our approach enables large-scale PICs to scale seamlessly beyond the single-reticle limit. © 2021 Optical Society of America

<https://doi.org/10.1364/OL.427289>

While major progress in the interconnect bandwidth of photonic integrated circuits (PICs) has been driven by increasing modulation rates, further improvement in bandwidth will require spatial, spectral, and polarization multiplexing [1,2]. Indeed, a recent demonstration with 1.6 Tbit/s capacity used 16 parallel 100 Gbit/s lanes [3]. As each lane needs a driver, modulator, and fan-out for electrical and optical connections, future higher-capacity optical interconnects will occupy even larger chip areas. Similarly, switches [4], optical phased arrays (OPAs) [5,6], quantum circuits [7], and tensor cores [8] have all demonstrated optical systems with component counts from several hundreds to tens of thousands, and will grow in area as their capabilities improve. The need for large chips is especially acute for ultralow-loss photonic platforms [9,10], which are desirable for microwave photonics [11,12], nonlinear optics [9], and gyroscopes [13–15]. These platforms may have bend radii of 1 mm or larger [9], and often require PICs at the centimeter scale.

The availability of 300 mm substrates in silicon foundries and the relatively large dimensions of PIC components enable PICs to be fabricated at low cost and high volume using prior-generation process nodes. Thus, increasing the area of PICs to the size of a reticle and beyond is an economical way to continue to scale performance. In Table 1, we estimate performance as die size grows to multiple reticles. With switch bandwidths projected to reach 51.2 Tbit/s by 2024 [2], the footprint of

interconnect PICs interfacing with those switches may soon surpass a single reticle. An 8192 element active OPA spanned an entire reticle [6]. Optical switches [4] and gyroscopes [15] have already reached multiple reticles, while a photonic quantum computer could achieve quantum supremacy in a system spanning three reticles [7]. The need for multi-reticle PICs motivates us to seek a stitching method optimized for photonics.

Multi-reticle exposures have already been used in electronic circuits for large-scale phased-array antennas and image sensors. Misalignment of exposures normal to the reticle boundary (x direction in Fig. 1) can lead to a gap between reticles, and is addressed by overlaying the adjacent reticles by a distance L larger than the alignment tolerance [Fig. 1(a)]. Lateral misalignment δ (y direction) causes an abrupt step in the sidewall as the waveguide crosses the reticle boundary. Deep-UV stepper alignment error of tens of nanometers [16] has little impact on all but the narrowest electronic wires, but such sidewall discontinuities lead to appreciable loss in photonic waveguides.

We propose enlarging the overlay distance and widening the waveguides as they traverse the stitch length L , which results in a seamless transition [Fig. 1(b)]. To design for alignment tolerance δ_{MAX} , the waveguide in each reticle widens linearly by $2\delta_{\text{MAX}}$ as it traverses the stitch length, L . The angle of the sidewall with respect to the propagation axis is $\theta = \tan^{-1}(\delta_{\text{MAX}}/L) \approx \delta_{\text{MAX}}/L$. Our scheme applies to a positive photoresist, in which exposed areas (indicated by hatching) are dissolved in developer and etched to form the waveguide. For a negative resist, each waveguide should instead be narrowed. In the case of perfect alignment [Fig. 1(c)], the waveguide widens and then narrows in the stitch region. For misalignment half of the alignment tolerance [Fig. 1(d)], the waveguide widens at the beginning of the stitch region and narrows at the end, as in the previous case. However, the width of the waveguide in the center of the stitch is constant, with propagation direction tilted from the input and output waveguides by the angle θ . For misalignment equal to the alignment tolerance [Fig. 1(e)], the waveguide width is constant throughout the stitch region, and angles by θ with respect to the input and output waveguides. Thus, the lateral misalignment is accommodated by a corresponding length of the waveguide with offset angle θ . The widening of the waveguide should be adiabatic enough that mode conversion loss is negligible, so the loss of the stitch can be entirely attributed to the junctions at either end of the angled waveguide, where the propagation direction changes and the phase fronts of the waveguide modes are misaligned. Accordingly, we refer to

Table 1. Multi-Reticle Performance of Integrated Optical Systems^a

	# of Reticles		
	1	2 × 2	4 × 4
Interconnect bandwidth (Tbit/s)	40	160	640
Optical switch (2D) radix	180 × 180	360 × 360	720 × 720
Optical neural network size (neurons)	470	1900	7500
Quantum circuit mode count (qubits)	21	43	86
OPA (2D, passive) emitters	5,000,000	20,000,000	80,000,000
OPA (1D, active) emitters	5000	20,000	80,000
Delay line length (m)	6	25	100
Gyroscope scale factor ((°/h)/μrad)	180	23	2.8

^aWe assume single-reticle size 2 cm × 2 cm. Interconnect bandwidth based on bandwidth density 100 Gbit/(s mm²) [3]. Switch radix based on 110 μm × 110 μm unit cell [4]. Neural network, quantum circuit size based on density of 2450 phase tuners per 21 cm² [7]. Passive 2D OPA size based on 4096 emitters per 576 μm × 576 μm [5]. Active 1D OPA emitter density based on an 8192 emitter chip [6]. Delay line length, gyroscope scale factor (rotation rate per Sagnac phase) based on Archimedes spiral of 50 μm pitch, 1 mm minimum bend radius [13].

the stitched waveguide in Fig. 1(a) as an “abrupt” stitch, and our optimized design in Fig. 1(b) as an “angled” stitch consisting of two “angled” junctions.

We validate our design using 100 nm thick silicon nitride waveguides in a CMOS-foundry ultralow-loss photonic platform [9]. Prior work in a similar platform [14,15] for which 0.1 dB/m loss is achievable [10] demonstrated abrupt stitching junctions with an estimated loss of 0.006 dB/stitch, contributing around 0.2 dB/m to the total loss in a 3 m delay line. We demonstrate our improved stitching method by fabricating stitched delay lines 23 m in length with an order-of-magnitude lower stitching loss [Fig. 2(a)]. In our design, the input to the stitch is a single-mode waveguide of 2.8 μm width. We select

δ_{MAX} of 300 nm, so that the waveguide widens to a width of 3.4 μm at the edge of the reticle. When exposed, adjacent reticles are overlaid by 500 μm. We design structures with stitch lengths L of 20, 100, and 450 μm. We observe a lateral misalignment below 20 nm on the fabricated wafer [Fig. 2(b)], so we use mask bias to apply additional misalignment (y direction) of $-100, 0,$ and 100 nm for each stitch length. We fabricate a stitched racetrack resonator for each configuration [Fig. 2(c)]. The resonator transmission spectra were measured and fitted to determine the resonator round-trip loss, and compared to a control device from the same die, consisting of a non-stitched resonator of identical dimensions. Any excess round-trip loss of the stitched devices versus the control device was attributed to the stitch design. The control device features an intrinsic Q factor of 45 M and round-trip loss of 0.005 dB at 1550 nm wavelength, allowing us to measure very low stitching losses. The measured data are presented in Fig. 2(e). For 20, 100, and 450 μm stitch lengths, the mean stitching losses, averaged over ± 100 nm bias and spectral range 1510–1600 nm, are 0.0167, 0.0014, and 0.00041 dB, with standard deviations of the means 0.0003, 0.00008, and 0.00004 dB, respectively. The measured loss of 0.0004 dB/stitch represents an order-of-magnitude improvement compared to prior work [4,15].

We compare our measured results with simulation. Rather than simulate the full structure, we observe that for short stitch lengths, we expect input and output waveguide modes to couple directly through the near field such that the loss approaches that of an abrupt junction, which we simulate by the modal overlap of the input and output waveguides with 100 nm alignment error. For large stitch lengths, the stitch is modeled by two junctions of waveguides with propagation directions differing by θ , which we calculate by finite-difference-time-domain simulation. The waveguide width of the stitch at the angle junction tapers up to δ_{MAX} wider than the input waveguide (W) depending on the misalignment, but $\delta_{\text{MAX}} \ll W$, so the dependence of loss on misalignment is small. The waveguide width at the junction is simulated as $W + \delta_{\text{MAX}}$, which provides a tight upper bound on the loss. The results of these two models are plotted with the measured stitching loss [Fig. 2(f)]. The loss of the 20 μm device agrees with the abrupt junction model, whereas the losses of the 100 and 450 μm devices agree with the angled junction model. Indeed, this suggests for a given misalignment (in this case, ± 100 nm) that the abrupt junction model imposes a maximum loss for the stitched waveguide, that

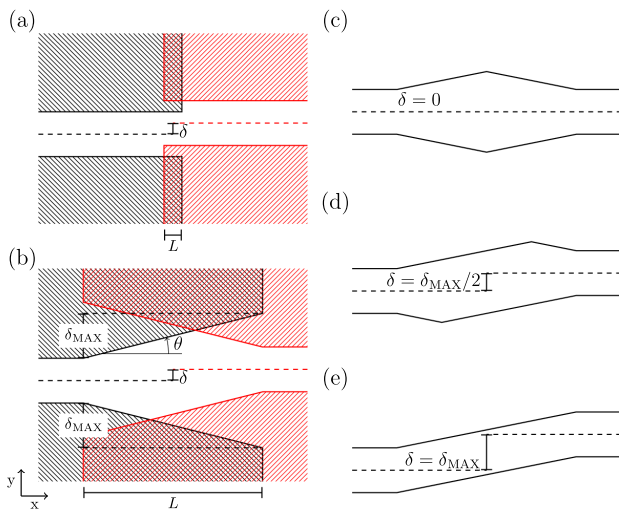


Fig. 1. Optimized stitching method. (a) Plan-view of un-optimized stitched waveguide between adjacent reticles. Black (red) hatched areas indicate regions exposed by the left (right) reticle; the waveguide is defined by the remaining unexposed areas; the dashed lines indicate the centers of the respective waveguides; δ indicates the lateral alignment error. (b) Instead, widening the overlaid waveguides over a larger distance L results in a continuous sidewall; the angle of the sidewall to the propagation axis is given by θ ; the waveguides widen by $2\delta_{\text{MAX}}$ yielding alignment tolerance δ_{MAX} ; regions with both black and red hatching are exposed by both reticles. (c) The stitched waveguide’s plan-view profile varies from (c) zero misalignment to (d) intermediate misalignment to (e) maximum tolerable misalignment.

is, the abrupt junction model is valid for stitch lengths below the point at which the models intersect (here, 35 μm), while the angled junction model is valid above it. The data in Fig. 2(e) are

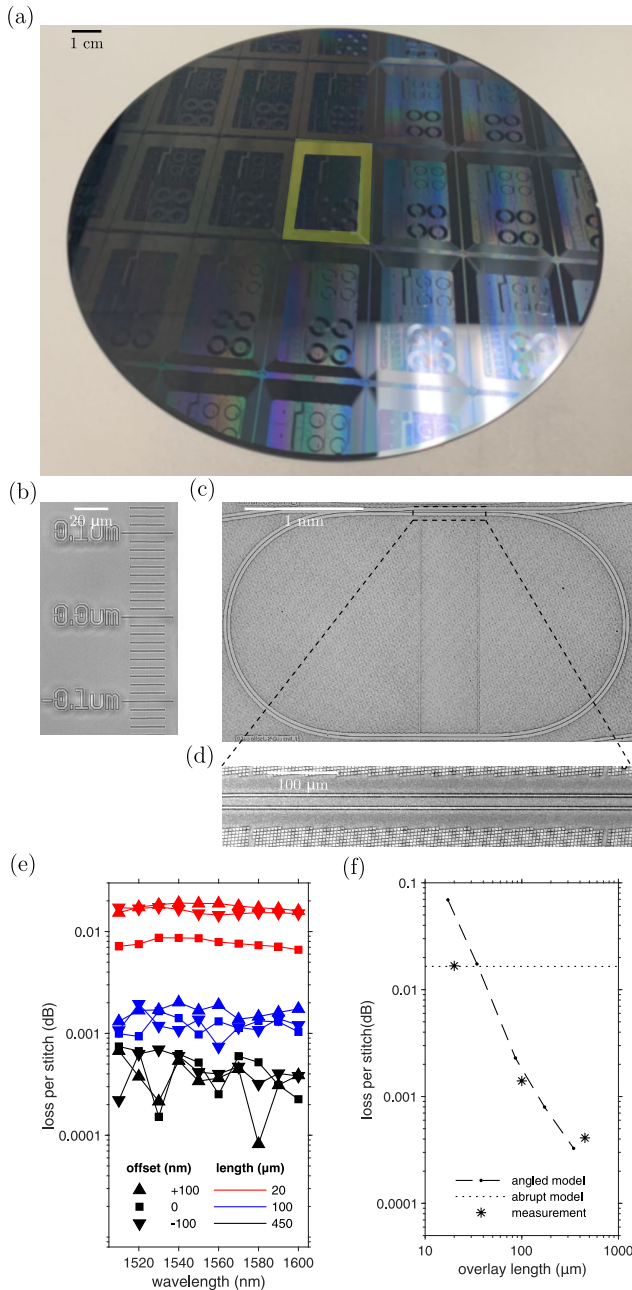


Fig. 2. Device measurement and model validation. (a) Fabricated 200 mm wafer with stitched delay lines 23 m in length on the perimeter of each die. The delay line of the center die is highlighted. Each die consists of two stitched reticles. The interior of each die is occupied by test structures. (b) Micrograph of alignment test structure between adjacent reticles. Each half of the mark is exposed separately; each mark represents an additional 10 nm alignment bias between left and right reticles. We estimate an alignment error below 20 nm. (c) Stitched racetrack resonator test structure. (d) Micrograph of stitched waveguides in a resonator. (e) Measured stitching loss versus wavelength for each test structure. Nine configurations were measured, consisting of three different stitch lengths, each evaluated for three mask offsets. (f) Comparison of measurement with simulation of our design at ± 100 nm misalignment.

consistent with this interpretation: the loss in an abrupt junction should vary with the alignment error, and the loss in the 20 μm long stitch indeed exhibits the lowest loss for 0 nm alignment bias. On the other hand, we expect the loss in the angled junctions to depend only on the angular misalignment $\theta \approx \delta_{\text{MAX}}/L$, independent of the alignment error δ . Accordingly, the measured losses in 100 and 450 μm long stitches do not depend on alignment bias.

We use our validated model to compare the performance of a seamless “angled” stitching method to the typical “abrupt” stitching method. Indeed, other authors [4] have employed abrupt stitching of 10 μm wide waveguides to achieve loss of 0.004 dB/stitch. While the abrupt stitch itself occupies zero length, the mode converters on either side of the stitch must be included in the length as well. We calculate the necessary length according to Milton and Burns [17] $L = n_{\text{eff}} W_{\text{MAX}}^2 / \alpha \lambda$, where L is the total length of the abrupt stitch including two mode converters, W_{MAX} is the width of the waveguide at the abrupt stitch, n_{eff} is the effective index of the mode at the stitch, $\alpha = 1$ is a scaling factor unity or lower for low loss, and $\lambda = 1550$ nm is the wavelength. The loss of the stitch is then calculated by mode overlap at the wide-waveguide abrupt junction. For simplicity, the conversion from single-mode to multimode is assumed lossless. In Fig. 3(a), we compare the abrupt stitch loss to the angled stitch loss for an alignment error of 100 nm. In the angled stitch design, we retain the 2.8 μm silicon nitride waveguide width at the stitch input and output, but choose δ_{MAX} of 100 nm. This reduction of δ_{MAX} from 300 nm in measured devices to 100 nm still represents a conservative alignment error, since a 3σ value of alignment error below 18 nm is achievable for deep-UV stepper lithography [16]. The abrupt stitch loss is simulated up to a waveguide width of 10 μm . For stitch length beyond 12 μm , the angled stitch outperforms the abrupt stitch.

To demonstrate the generality of the approach, we also consider widely available, 220 nm thick, deeply etched silicon

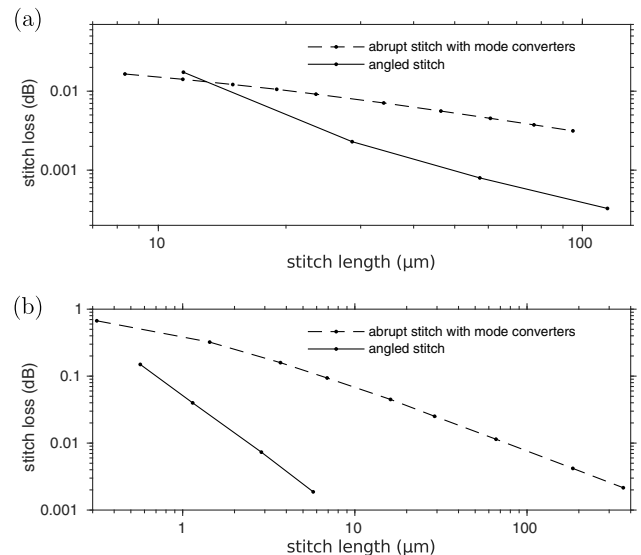


Fig. 3. Simulated loss versus length of “abrupt” and “angled” stitching at 100 nm alignment error for (a) 100 nm thick silicon nitride waveguides and (b) 220 nm thick silicon waveguides. To compare the loss and length of abrupt stitches with angled stitches, abrupt stitch loss is simulated as a function of waveguide width, while the length is calculated as the length of the corresponding mode converters for each waveguide width.

channel waveguides. In this stitch design, we adopt a 400 nm single-mode waveguide width at the input and output of the stitch, δ_{MAX} of 100 nm, and we again simulate the performance of our design as a function of stitch length L [Fig. 3(b)]. The abrupt stitch loss is simulated up to a waveguide width of 14 μm . Our optimized design in this silicon waveguide platform approaches 0.001 dB per stitch for a stitch length below 10 μm , compared to over 50 μm in the silicon-nitride-based design. We attribute this reduction to the narrower waveguide width of 400 nm, compared to 2.8 μm . This is because a narrower optical mode, for the same angle θ , accumulates less phase error across its width due to the mismatched phase fronts at the angled junction. At a stitch length of just 6 μm , our silicon waveguide stitch design achieves approximately 50-fold lower loss for the same length, or approximately 50-fold smaller footprint at the same level of loss, compared to the abrupt stitching approach.

In conclusion, we presented a novel method for stitching photonic waveguides to enable seamless transitions between reticles. We demonstrated in both simulation and experiment that it produces stitched waveguides with a smaller footprint and lower loss by over an order of magnitude compared to prior approaches. For delay lines and interferometric gyroscopes where the waveguide crosses a stitching boundary multiple times per round trip, ultralow stitching loss is critical. In our 23 m long device, the 332 stitches contribute just 0.13 dB to the total loss. However, for optical switch and interconnect applications, no signal path should cross a stitching boundary more than a handful of times, so the small stitch footprint is more valuable. Indeed, an abrupt stitch limits the pitch of waveguides crossing the reticle boundary to a value above the waveguide's width—over 10 μm in prior works [4]. In our approach, the width of the stitched waveguide can be kept close to the single-mode width, allowing a high density of waveguides to traverse reticles. Furthermore, while our approach was developed for the case of deep-UV stepper lithography in a foundry context, we note that it could be applied to the contact, i-line stepper, and even E-beam lithography tools that are common in research contexts.

Initially driven by demand for low-cost interconnects for datacenter networks and high-performance computing, PIC performance and scale have grown dramatically in recent years. Large-scale devices have emerged: high-radix optical switches; OPAs for LiDAR, free-space communications, and augmented/virtual reality displays; meshed interferometer networks for artificial intelligence, machine learning, and quantum computation; and ultralow-loss delay lines and resonators for nonlinear optics and metrology. Many of these applications have already demonstrated PICs at or beyond the single reticle limit, and will continue to grow as fabrication yields improve. We believe the low-loss multi-reticle PIC will soon become a critical tool in the optical system designer's toolbox.

Funding. DARPA LUMOS (HR001-20-2-0044); Anello Photonics.

Disclosures. WJ: Anello Photonics (E,I,P). AF, MP: Anello Photonics (I,E,P). JB: Anello Photonics (F).

Data Availability. Data underlying the results presented in this paper are not publicly available at this time but may be obtained from the authors upon reasonable request.

REFERENCES

1. N. Margalit, C. Xiang, S. M. Bowers, A. Bjorlin, R. Blum, and J. E. Bowers, *Appl. Phys. Lett.* **118**, 220501 (2021).
2. B. Buscaino, E. Chen, J. W. Stewart, T. T. Pham, and J. M. Kahn, *J. Lightwave Technol.* **39**, 1984 (2020).
3. S. Fatholouloumi, D. Hui, S. Jadhav, J. Chen, K. Nguyen, M. Sakib, Z. Li, H. Mahalingam, S. Amiralizadeh, N. N. Tang, H. Potluri, M. Montazeri, H. Frish, R. A. Defrees, C. Seibert, A. Krichevsky, J. K. Doylend, J. Heck, R. Venables, A. Dahal, A. Awujoola, A. Vardapetyan, G. Kaur, M. Cen, V. Kulkarni, S. S. Islam, R. Spreitzer, S. Garag, A. Alduino, R. Chiou, L. Kamyab, S. Gupta, B. Xie, R. Appleton, S. Hollingsworth, S. McCargar, and Y. Akulova, *J. Lightwave Technol.* **39**, 1155 (2021).
4. T. J. Seok, K. Kwon, J. Henriksson, J. Luo, and M. C. Wu, *Optica* **6**, 490 (2019).
5. J. Sun, E. Timurdogan, A. Yaacobi, E. S. Hosseini, and M. R. Watts, *Nature* **493**, 195 (2013).
6. C. V. Poulton, M. J. Byrd, B. Moss, E. Timurdogan, R. Millman, and M. R. Watts, in *Conference on Lasers and Electro-Optics (CLEO): Applications and Technology* (OSA, 2020), paper JTh4A-3.
7. J. Arrazola, V. Bergholm, K. Brädler, T. Bromley, M. Collins, I. Dhand, A. Fumagalli, T. Gerrits, A. Goussev, L. Helt, J. Hundal, T. Isacsson, R. Israel, J. Izaac, S. Jahangiri, R. Janik, N. Killoran, S. Sumar, J. Lavoie, A. Lita, D. Mahler, M. Menotti, B. Morrison, S. Nam, L. Neuhaus, H. Qi, N. Quesada, A. Reppingon, K. Sabapathy, M. Schuld, D. Su, J. Swinerton, A. Sava, K. Tan, V. Vaidya, Z. Vernon, Z. Zabaneh, and Y. Zhang, *Nature* **591**, 54 (2021).
8. J. Feldmann, N. Youngblood, M. Karpov, H. Gehring, X. Li, M. Stappers, M. Le Gallo, X. Fu, A. Lukashchuk, A. S. Raja, J. Liu, C. Wright, A. Sebastian, T. Kippenberg, W. Pernice, and H. Bhaskaran, *Nature* **589**, 52 (2021).
9. W. Jin, Q.-F. Yang, L. Chang, B. Shen, H. Wang, M. A. Leal, L. Wu, M. Gao, A. Feshali, M. Paniccia, K. J. Vahala, and J. E. Bowers, *Nat. Photonics* **15**, 346 (2021).
10. J. F. Bauters, M. J. Heck, D. D. John, J. S. Barton, C. M. Bruinink, A. Leinse, R. G. Heideman, D. J. Blumenthal, and J. E. Bowers, *Opt. Express* **19**, 24090 (2011).
11. C. G. Roeloffzen, L. Zhuang, C. Taddei, A. Leinse, R. G. Heideman, P. W. van Dijk, R. M. Oldenbeuving, D. A. Marpaung, M. Burla, and K.-J. Boller, *Opt. Express* **21**, 22937 (2013).
12. C. Xiang, M. L. Davenport, J. B. Khurgin, P. A. Morton, and J. E. Bowers, *IEEE J. Sel. Top. Quantum Electron.* **24**, 1 (2017).
13. S. Srinivasan, R. Moreira, D. Blumenthal, and J. E. Bowers, *Opt. Express* **22**, 24988 (2014).
14. S. Gundavarapu, M. Belt, T. A. Huffman, M. A. Tran, T. Komljenovic, J. E. Bowers, and D. J. Blumenthal, *J. Lightwave Technol.* **36**, 1185 (2018).
15. T. Huffman, M. Davenport, M. Belt, J. E. Bowers, and D. J. Blumenthal, in *IEEE Photonics Conference* (IEEE, 2016), pp. 478–479.
16. M. J. Van de Moosdijk, E. Van den Brink, K. Simon, A. Friz, G. N. Philipps, R. J. Travers, and E. Raaymakers, *Proc. SPIE* **4688**, 858 (2002).
17. A. Milton and W. Burns, *IEEE J. Quantum Electron.* **13**, 828 (1977).